

Supplementary Material

Transparent glassy composites incorporating lead-free anti-perovskite halide nanocrystals enable tunable emission and ultrastable X-ray imaging

Yakun Le,^{a,†} Xiongjian Huang,^{a,b,†} Hao Zhang,^a Zhihao Zhou,^a Dandan Yang,^a Bozhao Yin,^a Xiaofeng Liu,^c Zhiguo Xia,^a Jianrong Qiu,^d Zhongming Yang,^{a,b} Guoping Dong^{a, *}

^aSouth China University of Technology, School of Materials Science and Engineering, State Key Laboratory of Luminescent Materials and Devices, Wushan Road 381, Guangzhou, China, 510641

^bSouth China University of Technology, School of Physics and Optoelectronics, Wushan Road 381, Guangzhou, China, 510641

^cZhejiang University, School of Materials Science and Engineering, Yuhangtang Road 866, Hangzhou, China, 310058

^dZhejiang University, College of Optical Science and Engineering, State Key Laboratory of Modern Optical Instrumentation, Yuhangtang Road 866, Hangzhou, China, 310058

*Guoping Dong, E-mail: dgp@scut.edu.cn

[†]These authors contributed equally to this work.

Supplementary Note 1:

Tanabe-Sugano (T-S) diagrams can be used to describe the spectral characteristics of Mn²⁺ ions in different environments. By solving the T-S matrix, eqs (1-4) are obtained:^{48, 49}

$$B = \frac{94\alpha + \sqrt{49(T_2 - T_1)^2 - 768}}{49} \quad (\text{S1})$$

$${}^6A_1(S) \rightarrow {}^4A_1, {}^4E(G) = 10B + 5C + 20\alpha \quad (\text{S2})$$

$${}^6A_1(S) \rightarrow {}^4E({}^4D) = 17B + 5C + 6\alpha \quad (\text{S3})$$

$${}^6A_1(S) \rightarrow {}^4T_2(G) = -10Dq + 18B + 6C - (26B^2/10Dq) + 22\alpha \quad (\text{S4})$$

where T₁ and T₂ are energies of ⁶A₁(S)→⁴A₁, ⁴E(G) and ⁶A₁(S)→⁴E(⁴D) transitions derived from the excitation spectra (Fig. S4), α represents the stress correction coefficient and is set to 76 cm⁻¹.

Supplementary Note 2:

The photon with incident intensity of I_0 , penetrating the material with mass thickness of x and density of ρ , has an intensity of I , which is given by the exponential attenuation law:⁵⁰

$$I/I_0 = \exp[-(\mu/\rho)x] \quad (\text{S5})$$

Besides, x is defined as the mass thickness per unit area, obtained by the thickness t multiplied by the density ρ (i.e., $x = \rho t$). Therefore, eq 1 can be expressed as:

$$I/I_0 = \exp[-(\mu/\rho) \rho t] \quad (\text{S6})$$

For compounds such as BGO, CsPbBr₃ and Cs₃MnBr₅ NC-embedded glass, the value of mass attenuation coefficient, μ/ρ , can be obtained according to simple additivity:

$$\mu/\rho = \sum w_i (\mu/\rho)_i \quad (\text{S7})$$

where w_i is the fraction by weight of the i th atomic constituent, and the $(\mu/\rho)_i$ values of each atom can be obtained from the following URL:

<https://physics.nist.gov/PhysRefData/Xcom/html/xcom1.html>.

Table S1. The RL stability of some materials under X-ray excitation at high temperature.

Materials	Highest temperature (K)	Ratio to RL intensity@ RT (%)	Ref.
[TPPen]₂Mn_{0.9}Zn_{0.1}Br₄ single crystals@PDMS(polydimethylsiloxane)	383 K	85	51
Cs₅Cu₃Cl₆I₂ powder@PDMS	423 K	65	52
Cs₃Cu₂I₅ powder@PS(polystyrene)	433 K	7.5	53
Cs₃Cu₂I₅: Mn 10% powder@PS	433 K	71	53
Cs₃MnBr₅ NC-embedded glass	563 K	73	This work

1. Characterizations of Cs₃MnBr₅ NCs in the glass.

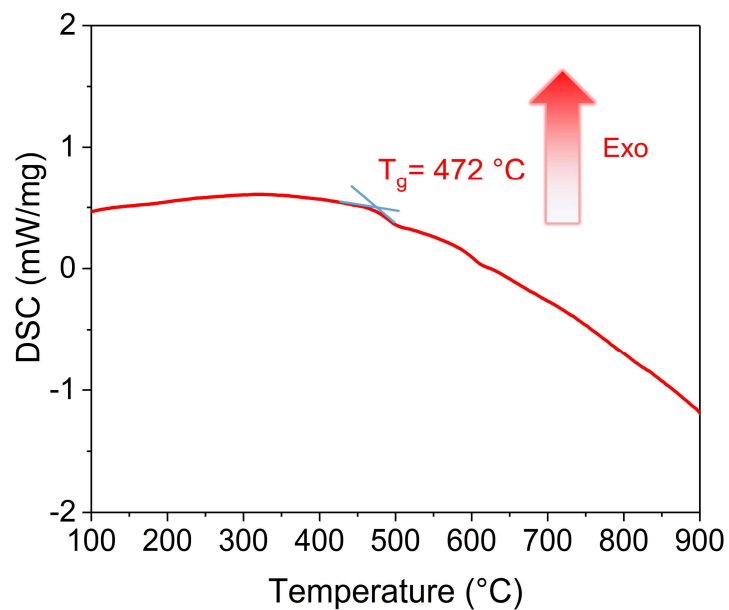


Fig. S1 Differential scanning calorimetry (DSC) curve of the PG. According to DSC, it can be found that the glass transition (T_g) temperature of the glass sample is 472 °C. Due to the small size and volume fraction of the Cs₃MnBr₅ NCs formed in the glass matrix, no obvious crystallization peak was observed. Therefore, we conducted a series of annealing procedures on the glass at temperatures higher than 490 °C.

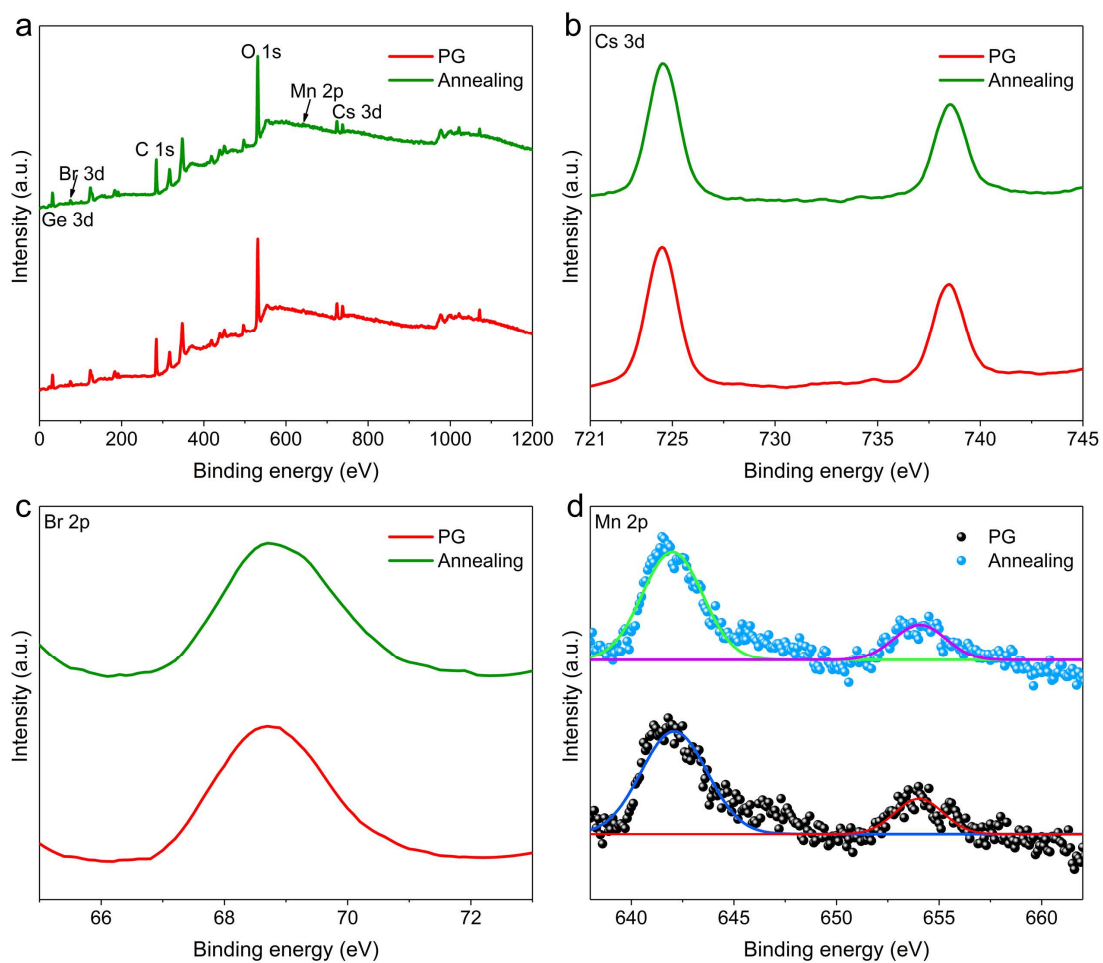


Fig. S2 (a-d) X-ray photoelectron spectroscopy (XPS) survey scan (a), and high-resolution XPS spectra of Cs (b),

Br (c) and Mn (d) for the PG and the glass sample annealed at 570 °C for 5 h.

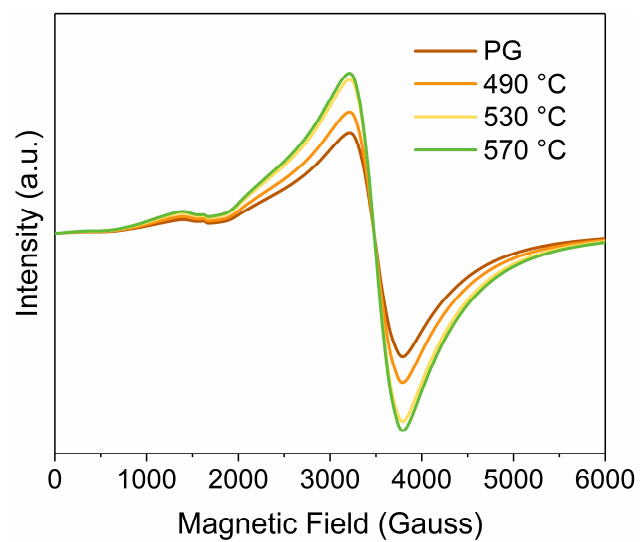


Fig. S3 EPR spectra recorded at room temperature for the glass sample annealed at different annealing temperatures.

2. PL properties of Cs₃MnBr₅ NCs in the glass.

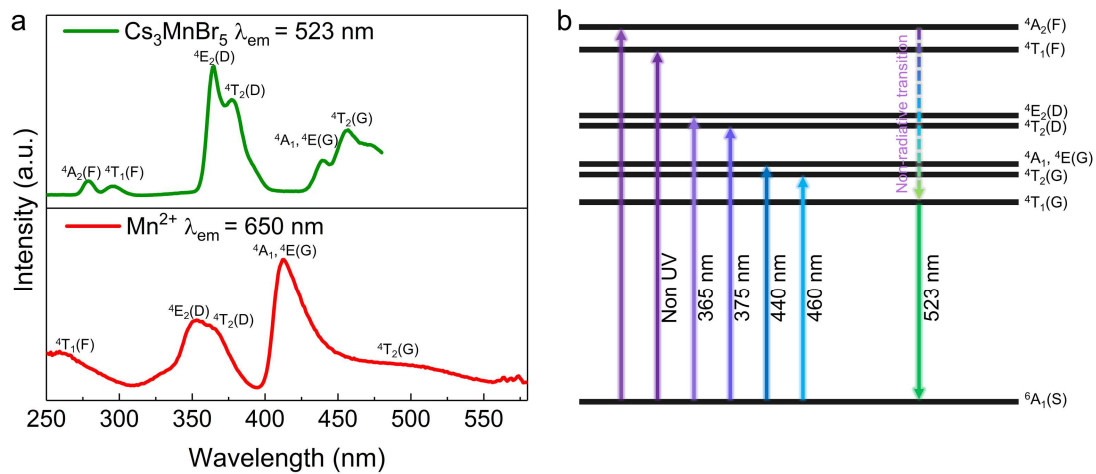


Fig. S4 (a) PLE spectra of Cs₃MnBr₅ NCs and Mn²⁺ ions in glass annealed at 570 °C for 5 h. (b) Schematic diagram

of the energy levels of Mn²⁺ ions in Cs₃MnBr₅ NCs.

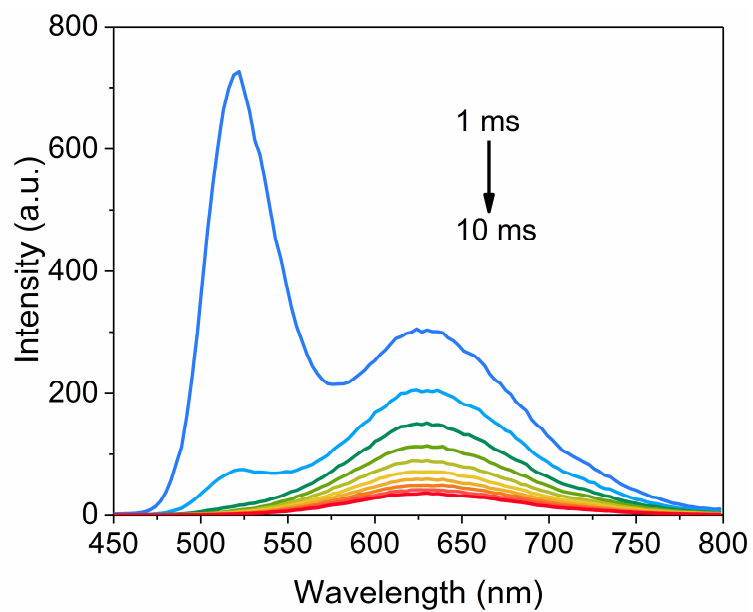


Fig. S5 Time-resolved PL spectra recorded from 1 ms to 10 ms following pulse excitation for the glass sample annealed at 570 °C for 5 h.

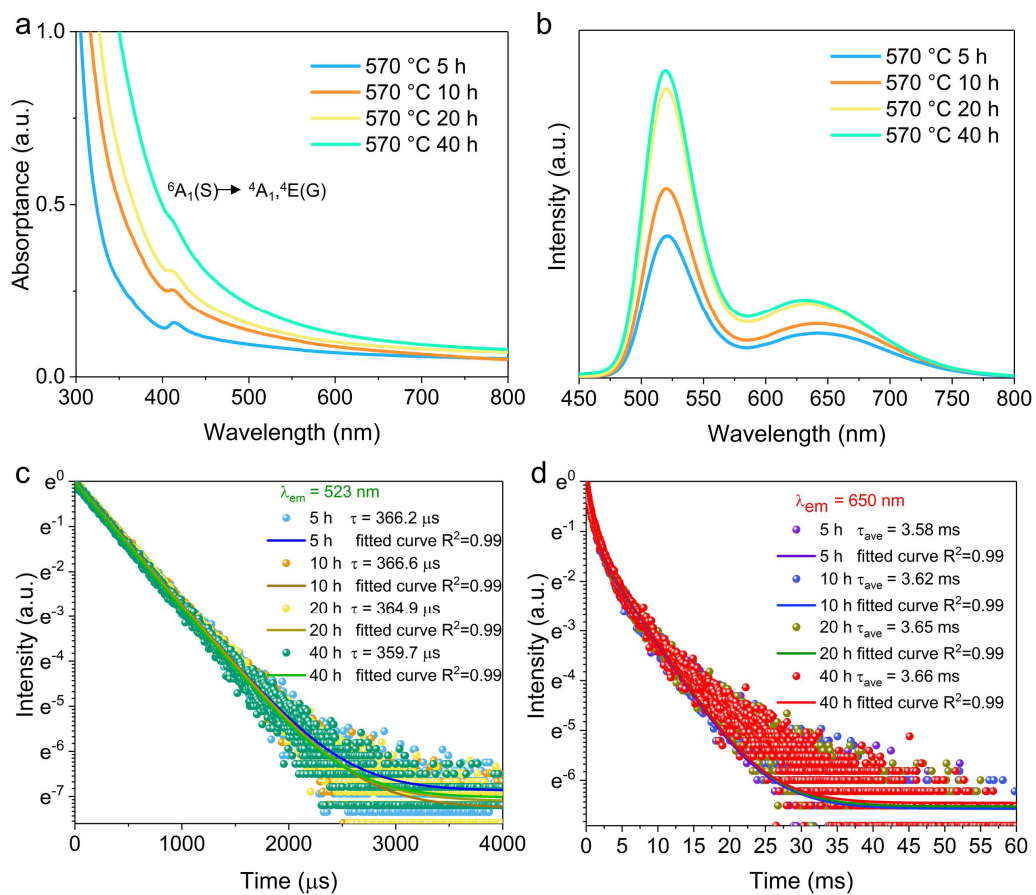


Fig. S6 (a-d) Absorption spectra (a), PL spectra (b) and PL decay curves of Cs₃MnBr₅ NCs (c) and Mn²⁺ ions (d) for the glass sample annealed at 570 °C for different durations. The fitting curves are fitted with single-exponential (c) and double-exponential (d), respectively.

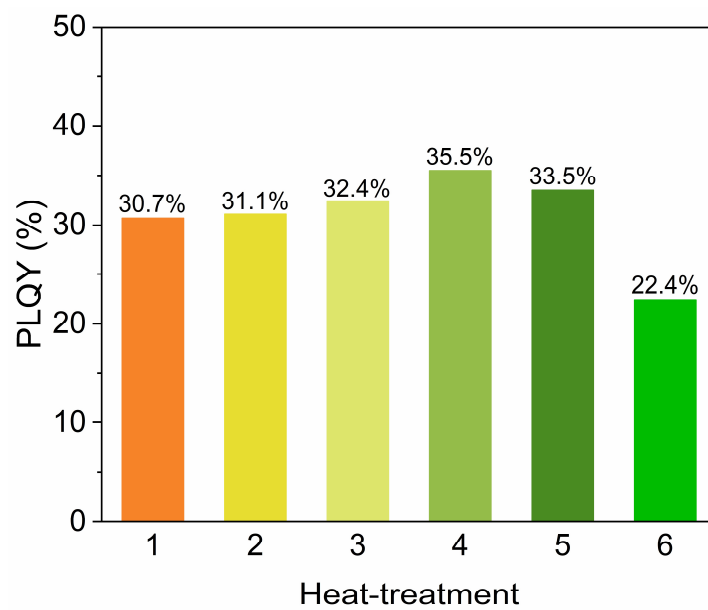


Fig. S7 PLQY recorded under 365 nm light excitation for the glass sample heat-treated at 490 °C (1) and 530 °C (2) for 5 h, and 570 °C for 5 h (3), 10 h (4), 20 h (5) and 40 h (6).

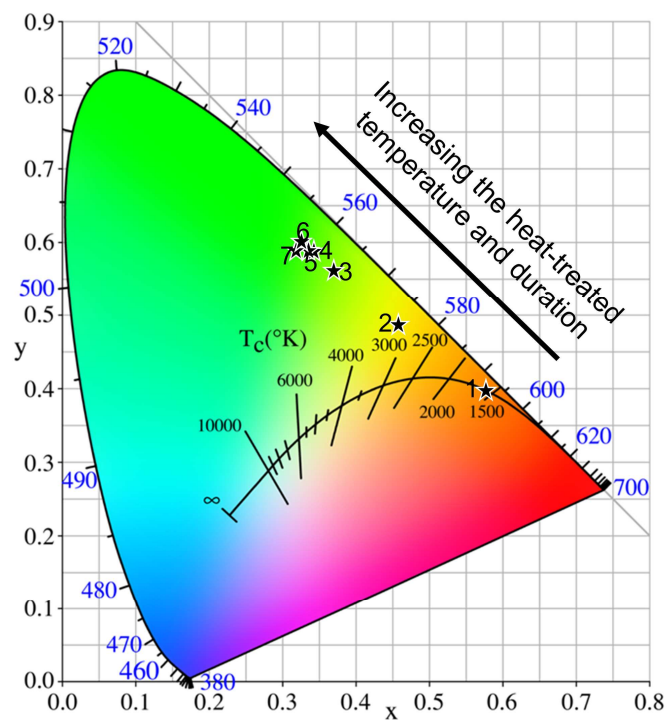


Fig. S8 Chromaticity coordinates for the PL from the glass samples heat-treated at various temperatures and durations. The excitation wavelength used in the Commission Internationale de L'Eclairage (CIE) 1931 diagram is 365 nm. The glass samples were heat-treated at 490 °C (1) and 530 °C (2) for 5 h, and 570 °C for 5 h (3), 10 h (4), 20 h (5) and 40 h (6).

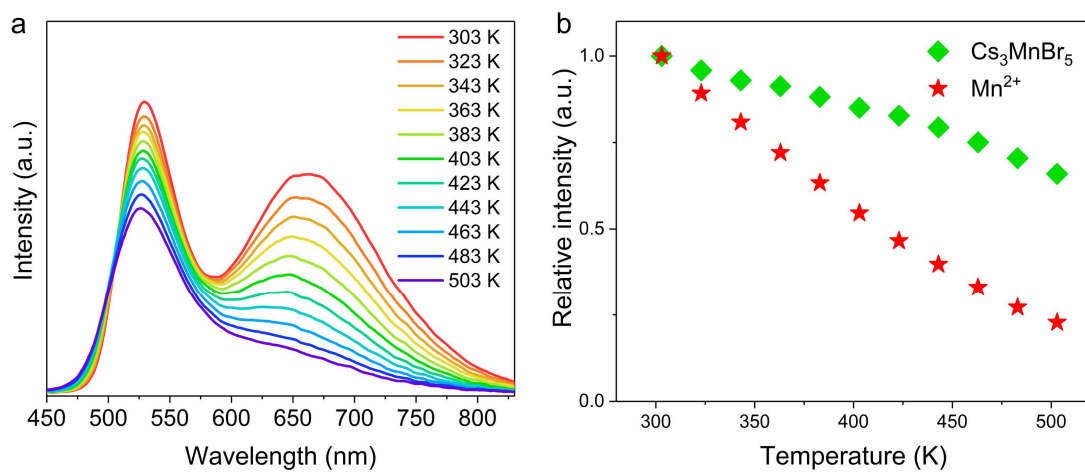


Fig. S9 (a, b) Temperature-dependent PL spectra (a) and emission intensity as a function of measurement temperature (b) for the glass sample annealed at 570 °C for 5 h under 375 nm laser excitation.

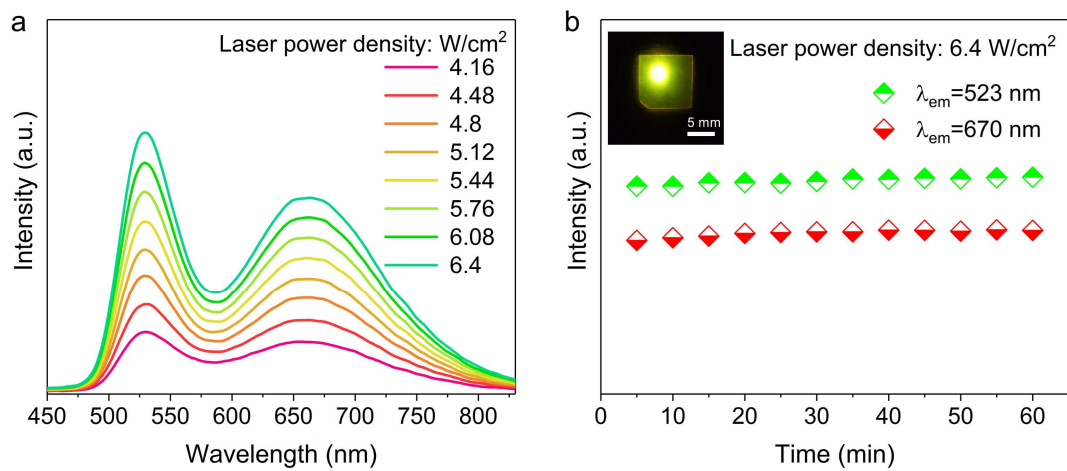


Fig. S10 (a) PL spectra of the glass sample annealed at 570 °C for 5 h at different laser power densities. (b) Time-dependent emission intensity of the corresponding sample under continuous excitation at 6.4 W/cm² power density for 1 h. The excitation wavelength used in (a, b) is 375 nm.

3. RL properties of Cs₃MnBr₅ NCs in the glass

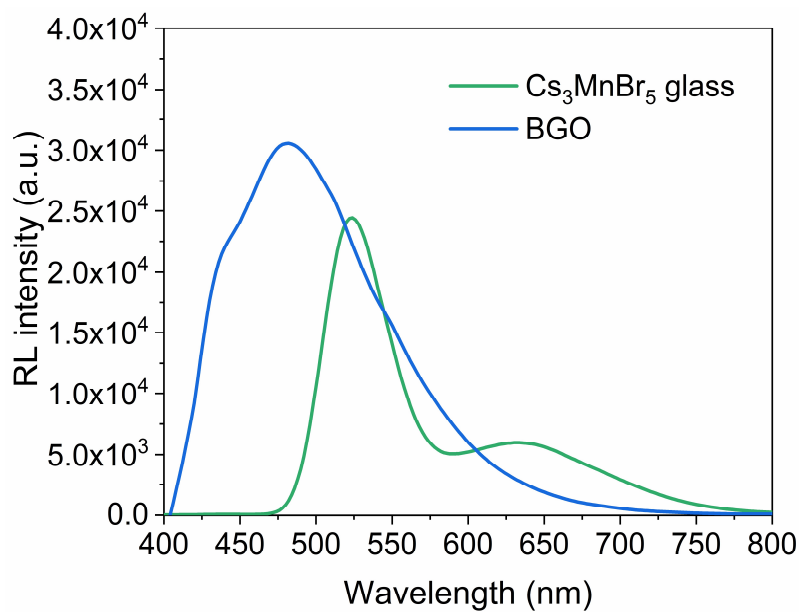


Fig. S11 RL spectra of BGO and Cs₃MnBr₅ NC-embedded glass. The light yield of BGO is ~ 10000 photons MeV⁻¹, therefore, the light yield of Cs₃MnBr₅ NC-embedded glass is estimated to ~ 5200 photons MeV⁻¹ by comparing their RL integral area.⁴²

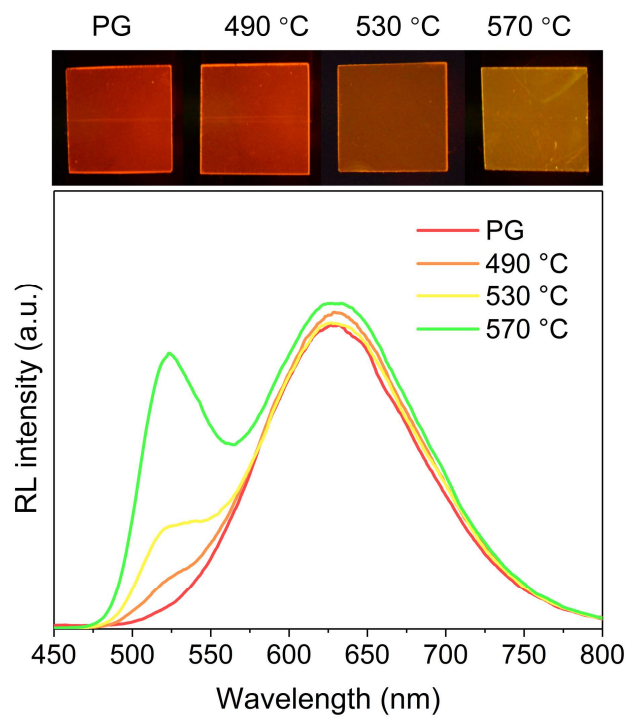


Fig. S12 Photographs (top) and RL spectra (bottom) of the PG and the glass sample annealed at different annealing temperatures for 5 h under X-ray excitation with a dose rate of $4.814 \text{ mGy}_{\text{air}} \text{ s}^{-1}$.

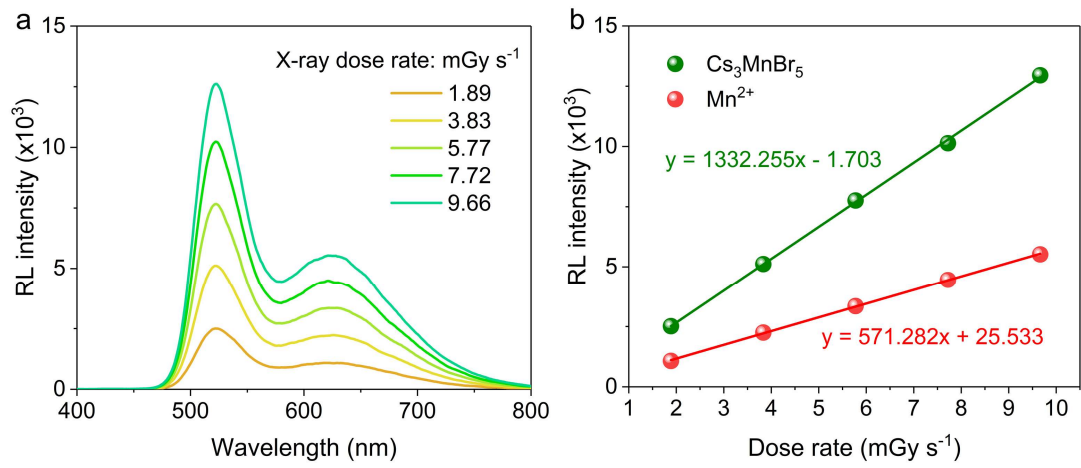


Fig. S13 (a, b) RL spectra (a) and liner relationship between dose rate and RL intensity (b) of Cs₃MnBr₅ NCs and

Mn²⁺ in glass at different dose rates under X-ray excitation.

4. The X-ray imaging performance of Cs_3MnBr_5 NCs encapsulated in the glass.

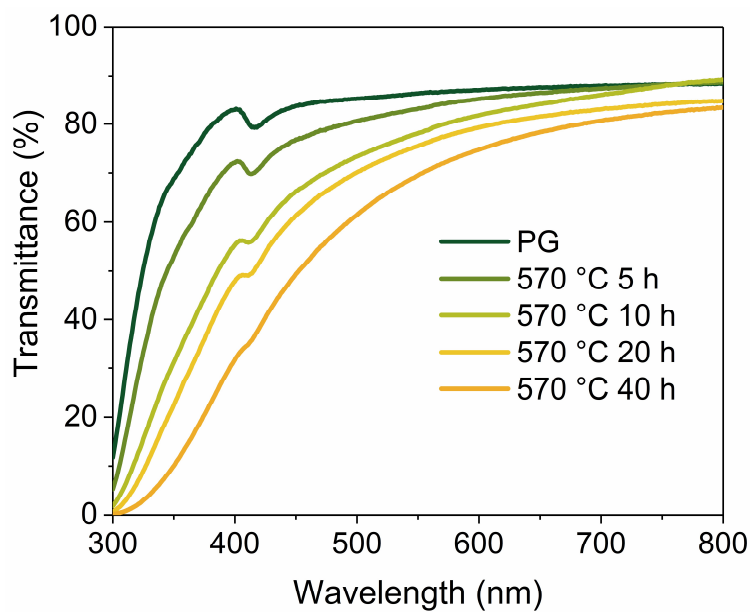


Fig. S14 Transmittance spectra of the glass samples annealed at 570 °C for different durations.

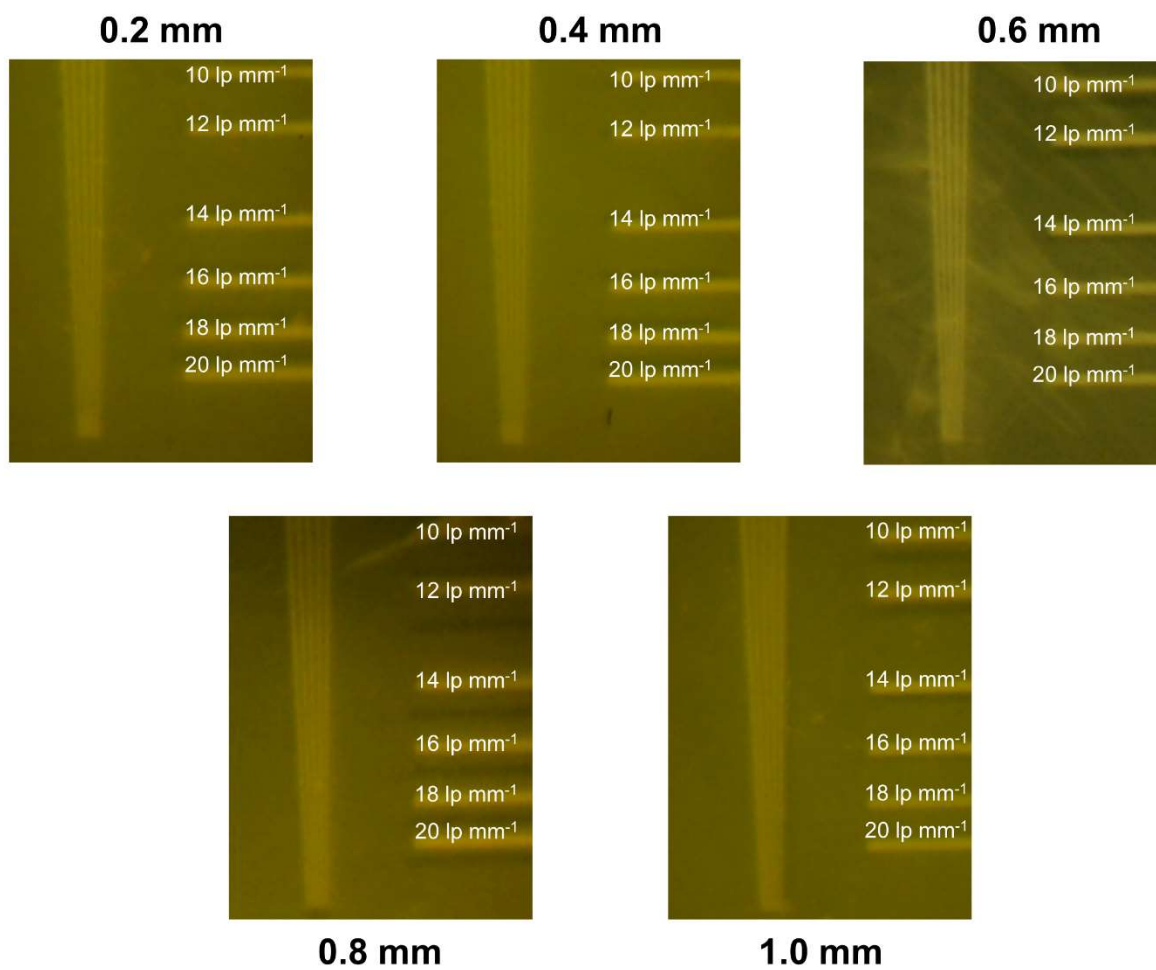


Fig. S15 X-ray images of the standard X-ray resolution pattern plate with different thicknesses of glasses.

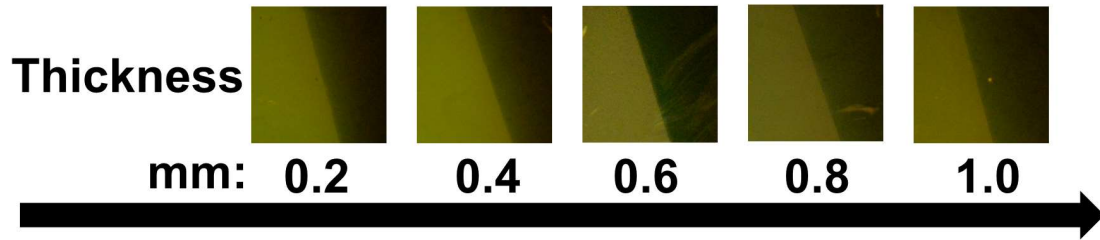
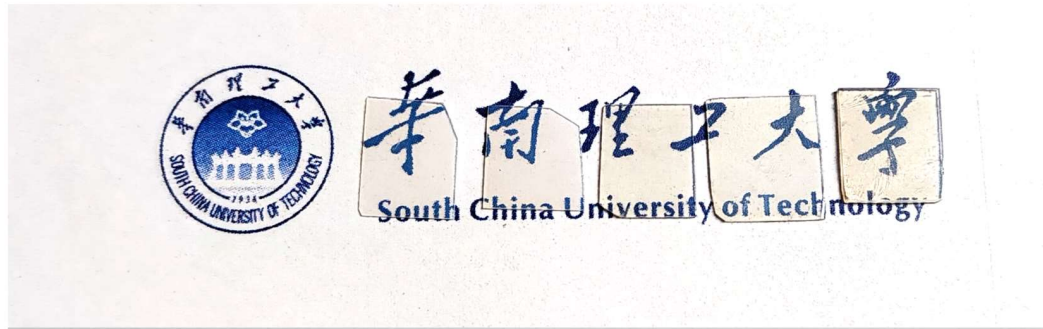


Fig. S16 Photographs of different thicknesses of glasses under daylight and modulated X-ray imaging, respectively.

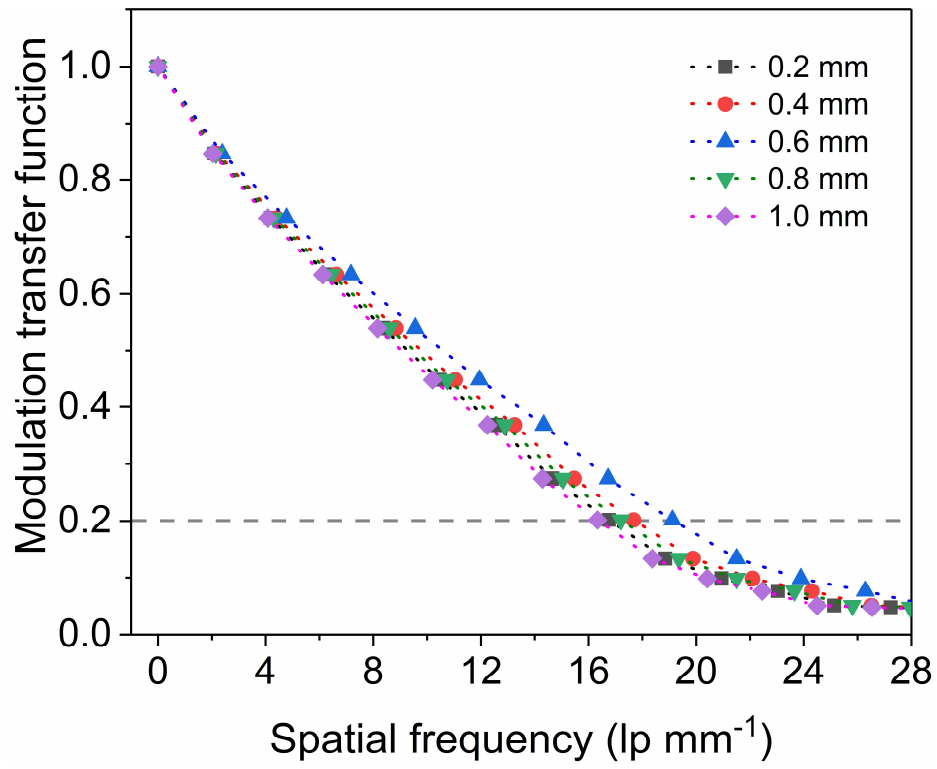


Fig. S17 MTF of X-ray images obtained from the different thicknesses of glasses.

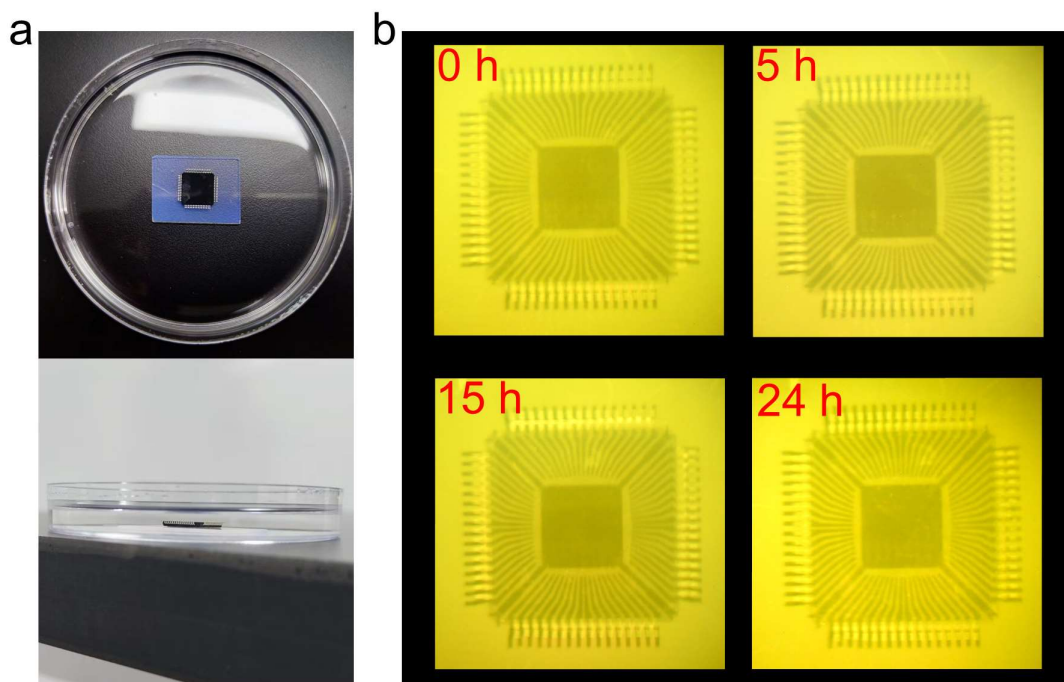


Fig. S18 (a) Top view (top) and side view (bottom) photographs of the AI chip and Cs_3MnBr_5 NC-embedded glass soaked in deionized water. (b) X-ray images of the AI chip in deionized water with storing times up to 24 h.

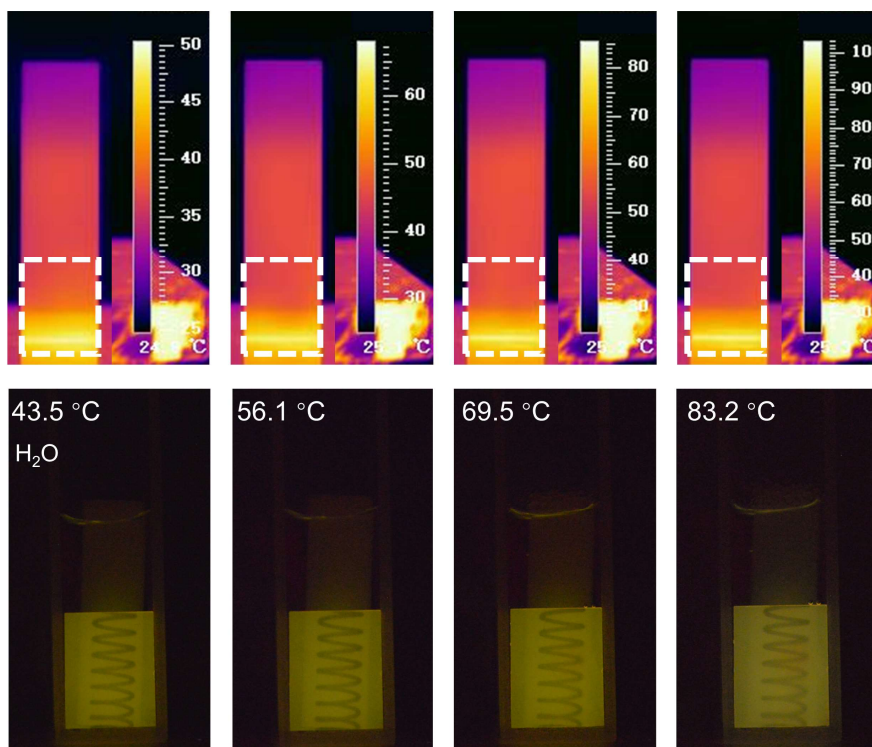


Fig. S19 Thermal imaging photographs (top) and X-ray images (bottom) of a cylindrical ABS resin embedded with an iron spring immersed in deionized water at different temperatures.

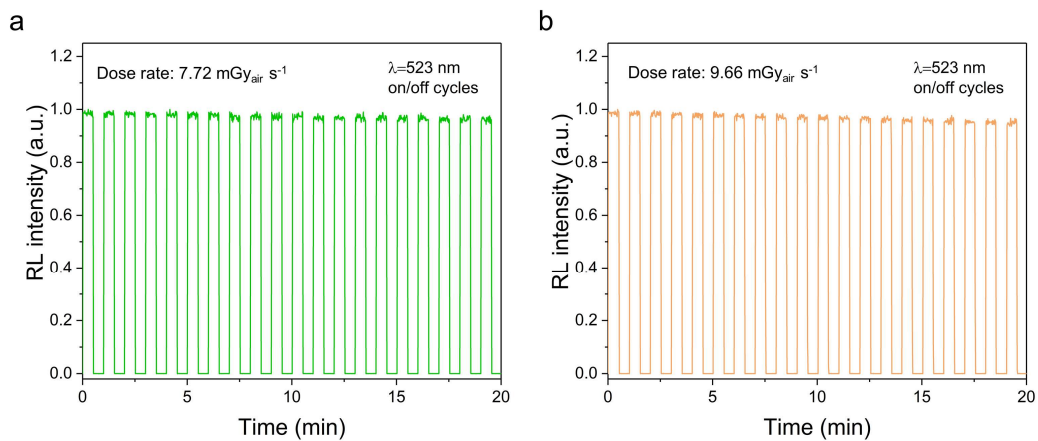


Fig S20 RL intensity of Cs₃MnBr₅ NCs in the glass recorded under different dose rates over continuous 20 on/off cycles during 20 min.

Video 1. real-time radiography was performed by recording the rotation procedure of an iron spring with an angular velocity of $\pi/12$ rad s⁻¹.